Lung Disease Detection using neural networks, a comparative study of models.

Leonard Eckhoff, Mayur Jaisinghani, Kaushik Shridhar
Department of Computer Science,
Indiana University Bloomington.

Abstract:

This paper delves into the intricate realm of neural network applications for lung disease detection, with a deliberate focus on conducting a comprehensive comparative analysis of various model architectures. Informed by a diverse dataset containing high-resolution X-ray images capturing nuanced manifestations of lung diseases, ranging from pneumonia to lung cancer, the research meticulously evaluates the performance and efficiency of different neural network models. This analysis focuses on key architectures, including convolutional neural networks (CNNs) [22], multilayer preceptrons (MLP) and pretrained models such as ResNet50 [23] and DenseNet 121 [24].

Introduction:

Deploying neural networks for the classification of medical images is a challenging task, due to the fact, that most clinical samples are by magnitudes smaller than usual datasets used to train multimillion parameter convolutional neural networks such as ResNet50 , MLP and CNN or Densenet 121. The task is further complicated that human anatomy is highly complex and variable and thus imposes a challenge to the generalization capabilities of models. Besides that medical imagery such as CT, MRI or X-Ray scans are often subject to very high nuisance due to patient movement and other technical artefacts. The lungs are affected by a lot of ailments like aortic enlargement, pulmonary fibrosis etc. Aim of this project is to compare multiple approaches to increase the predictive performance of these diseases.

Medical Background:

1. **Aortic enlargement:** Aortic enlargement, also referred to as aortic aneurysm is a bulge in the wall of the aorta, which is the largest/main artery from one's heart. It develops in a weak region of the arterial wall. The rupturing or splitting of enlarged aorta can lead to internal bleeding, block the flow of blood from heart to other organs and can prove to be fatal [1]. Aortic aneurysm can be detected via chest X ray through some crucial identifiable characteristics: the mediastinal silhouette appears to be widened, the aortic knob looks enlarged, or the trachea seems displaced from the middle [2].

Fig1: Chest radiograph showing widening of the superior mediastinum in case of thoracic aortic aneurysm [2].

2. **Atelectasis:** Atelectasis is a state of collapsed and non-aerated region of the lung parenchyma. It is connected to several pulmonary and chest disorders. It can occur via airway obstruction, compression of parenchyma by extrathoracic, intrathoracic chest

wall processes, and increased surface tension in alveoli and bronchioles. Anterior-posterior and lateral projections of the chest via radiography is necessary for the detection and documentation of this disorder [3]. It is observable as small volume linear shadows, usually peripherally or at the lung bases [4].

3. **Calcification:** Vascular calcification is highly correlated with cardiovascular disease mortality and is considered a marker of atherosclerotic plaque burden in addition to contributing loss of arterial compliance [5]. It is usually visible as nodules or masses [6].
4. **Cardiomegaly:** Cardiomegaly is an umbrella term used to describe various conditions which cause the enlargement of heart. Specifically, it refers to a condition when the transverse diameter of the cardiac silhouette is greater than or equal to 50% of the transverse diameter of the chest, resulting in increased cardiothoracic ratio. This morphological change can be observed via posterior-anterior projection of a chest radiograph [7].

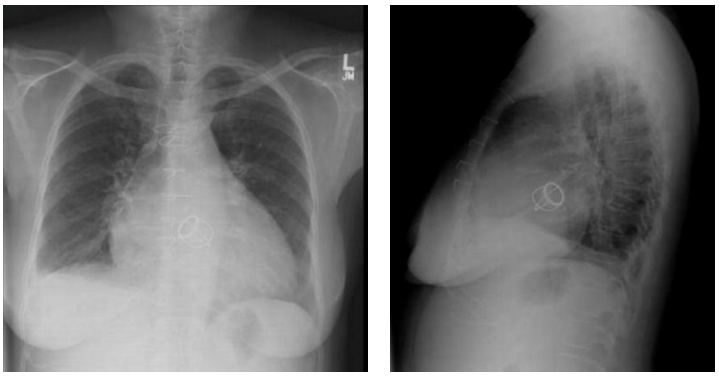

2(a) 2(b)

Fig 2: (a) Frontal and (b) lateral chest X-ray of a woman suffering from cardiomegaly [8].

5. **Lung Consolidation:** Lung consolidation occurs when fluid, solid, or other material—such as pus, blood, water, stomach contents, or cells—replaces the air in the lungs' narrow airways. A few possible cause for lung consolidation are lung cancer, pneumonia, and aspiration. If someone suffers from lung consolidation they would face difficulty in breathing which can result in lack of oxygen intake. This disorder is easily visible on chest x-rays where consolidated parts of the lung look white, or opaque [9].

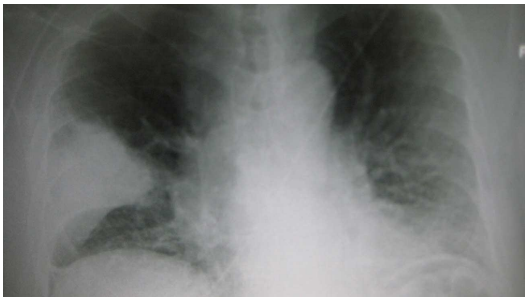

Fig 3: Case of pulmonary consolidation where the consolidated parts appear white.

6. **ILD:** Interstitial Lung Disease (ILD) refers to a broad category of illnesses that result in lung fibrosis, or scarring. In such cases, the ability to breath and get oxygen into circulation are hampered by the rigidity in the lungs caused by the scarring. ILD-related lung damage is frequently irreversible and worsens over time [10]. ILD can be visualised by x ray and it generally tends to cause infiltrative opacification in the periphery of the lung, but the patterns often varies [11].

7. **Infiltration:** Pulmonary infiltrate refers to a condition where an abnormal substance accumulates gradually within cells or body tissues or any foreign substance or type of cell spreads through the lung or accumulates in the lung over the normally observed quantity. Infiltrates appear as white spots in a chest x-ray [12].
8. **Lung opacity:** Normal lungs appear dark as compared to the surrounding area in a chest radiograph due to them being filled by air which has a lower density. However, when air in the lungs is replaced by fluid or fibrosis, the lungs become more dense and they appear more cloudy/light grey in the radiographs. Thus lung opacity refers to an area of the chest radiograph that is supposed to look darker but looks denser/light grey instead [13].

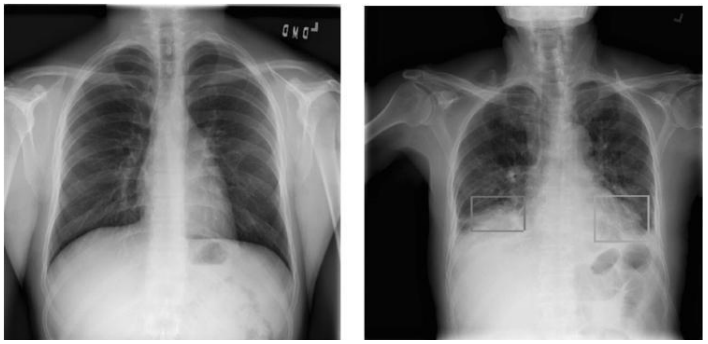

4(a) 4(b)

Fig4: (a) Lungs of a healthy individual (b) Lungs showing observable opacity in certain areas which are clear in healthy individuals as observed in 4(a). [13]

9. **Nodules/mass:** Small cell clusters in the lungs called lung nodules. They are quite prevalent and usually do not cause any symptoms. Majority of the lung nodules are remnants/ scar tissues from previous lung infections. They are usually begin but can also indicate lung cancer in some cases. Noldules that are larger than 3 cm are considered masses and are treated as cancerous until proven otherwise. They appear as small, rounded opacities within the lungs on chest radiographs [14].
10. **Pleural effusion:** Buildup of fluid in the pleural cavity, which lies between the parietal and visceral pleura, is known as pleural effusion. It may occur on its own or as a result of a parenchymal disease that surrounds it, such as an infection, cancer, or inflammatory disorders. It is one of the main causes of lung mortality and morbidity [15].

Fig 5: A case of massive pleural effusion with mediastinal shift [16].

11. **Pleural thickening:** Pleural thickening (PT) is the thickening of the lung lining as a result of scar tissue around it. The pleural lining serves to cushion the organs and provide a layer of protection for the lungs. Pleural thickening is visible on x rays as wedge-shaped apexes or deformed areas at the top portions of the lungs [17].
12. **Pneumothorax:** Pneumothorax commonly referred to as ‘collapsed lung’, occurs when air leaks into the gap between the lung and chest wall. This air pushes on the

outside of the lung and causes it to collapse. Pneumothorax refers to complete as well as partial lung collapse [18]. Pneumothorax is observable on erect chest radiographs as: Visceral pleural edge visible as a very thin, sharp white line; peripheral space is radiolucent compared to the adjacent lung; lung may have completely collapsed [19].

13. **Pulmonary fibrosis**: Pulmonary fibrosis is a lung disease wherein the tissue that surrounds the lungs' air sacs or alveoli sustains damage, thickens, and scars [20]. It can also be described as the development of excess fibrotic tissue in the lung. In case of pulmonary fibrosis, breathing becomes harder because of the lungs being stiffened and scarred. This might lead to a low oxygen supply to blood. The structural distortion of lungs on radiographs may indicate pulmonary fibrosis [21].

Technical Background:

1. **Related Work:**

   [25] presents multiple approaches for the detection of pneumonia using chest XRays. The Approaches so far can be categorized into CNN-based models, the use of pre-trained models as well as ensemble models. CNN-based models train the freshly intialized models and solely train them on XRay images; examples could be [26] or [27]. Transfer learning is an approach, which tries to utilize information, that was already learned on a source domain on a so called target domain. In the context of medical imagery image classification networks, which already have been trained on the ImageNet [28] - a large dataset containing more than 14 million annotated images belonging to over 20,000 categories. These models are hence already capable of feature detection and image classification. In order to deploy them on a target domain the vast majority of parameters gets frozen - i.e. they are not updated during the learning process - and the head of the model is either replaced or augmented with a new layer [29]. In [30] compared numerous image classification networks and their respective transfer capabilites.

2. **Image File Types: Dicom, JPG, RGB and Greyscale:**

- **DICOM (Digital Imaging and Communications in Medicine):** DICOM is a standard for transmitting, storing, and sharing medical images. It is widely used in the field of medical imaging, including X-rays, CT scans, and MRIs. DICOM files not only contain the image data but also include metadata such as patient information, imaging parameters, and annotations. This format ensures interoperability among different medical imaging devices and systems.
- **JPG (Joint Photographic Experts Group):** JPG, or JPEG, is a widely used image compression format. It is suitable for photographs and images with continuous tones and gradients. JPG files use lossy compression, meaning some image data is lost during compression to reduce file size. While it's not typically used for medical imaging due to lossy compression, it is commonly used for general-purpose imaging and on the web.
- **RGB (Red, Green, Blue):** RGB is a color model used in digital imaging. In the RGB model, colors are represented by combining different intensities of red, green, and blue light. Each pixel in an RGB image is composed of three color channels. This format is common for general-purpose color images and is widely used in applications such as photography and computer graphics.
- **Greyscale:** Greyscale, or grayscale, images use shades of grey to represent different levels of intensity or brightness. Unlike RGB images, greyscale images have only one channel, where each pixel's value corresponds to its intensity. Greyscale images are

often used in medical imaging, where color information may not be necessary, and the focus is on variations in intensity, as seen in X-rays or certain types of microscopy.

3. **CNNs and MLPs:**

   Convolutional Neural Networks (CNNs) and Multilayer Perceptrons (MLPs) represent two distinct yet powerful paradigms in the realm of lung disease detection. CNNs, renowned for their effectiveness in image processing tasks, excel at capturing intricate spatial features within medical images. Their hierarchical architecture, characterized by convolutional layers followed by pooling layers, enables automatic extraction of complex patterns, crucial for identifying subtle abnormalities in lung scans. CNNs are particularly adept at discerning local patterns, making them invaluable for tasks like nodule detection or tissue classification in lung images.

   On the other hand, Multilayer Perceptrons (MLPs), a fundamental type of artificial neural network, exhibit versatility in handling structured and tabular data. MLPs comprise interconnected layers of neurons, each layer capable of learning complex relationships within the input data. In the context of lung disease detection, MLPs can be applied to feature vectors derived from medical data, encompassing patient history, demographic information, and various clinical parameters. While lacking the spatial awareness inherent to CNNs, MLPs excel in learning non-linear relationships, making them proficient in synthesizing diverse information for accurate disease classification. The juxtaposition of CNNs and MLPs in lung disease detection underscores the significance of selecting an appropriate neural network architecture tailored to the nature of the data and the intricacies of the diagnostic task at hand.

   CNN is found to give slightly higher accuracy than MLP, but more research is needed to identify the architecture that gives better accuracy. [22]This paper compares Multi-Layer Perceptron Neural Network and Convolutional Neural Network for breast cancer diagnosis and classification. It then examines various researches that use Convolutional Neural Network for breast cancer detection. Convolutional neural network is better for complex image classifications, but MLP-NN shows higher accuracy in diagnosing and classifying breast cancer cells. Using artificial metaplasticity in MLP can help minimise error, but CNN shows results with higher accuracy.

4. **ImageNet:**

   Since we are using transfer learning [31], to try and compare the results, it is important to know about ImageNet dataset.

   ImageNet is a large-scale dataset containing millions of labeled images across thousands of classes. It was originally designed for object recognition tasks, where the goal is to classify images into specific categories. While ImageNet itself doesn't specifically focus on lung disease detection, it can still be useful in the context of training neural networks for medical image analysis, including lung X-ray datasets.

5. **ResNet50:**

   ResNet-50, short for Residual Network with 50 layers, is another powerful convolutional neural network (CNN) architecture that has been widely used for image classification tasks, including medical image analysis such as lung disease detection. The key innovation in ResNet-50 is the use of residual blocks. Traditional deep

networks can suffer from the vanishing gradient problem, making it challenging to train very deep models. Residual blocks address this by introducing skip connections or shortcuts. The output of a layer is added to the input, allowing the model to learn residual mappings.

6. **DenseNet 121:**

   DenseNet (Densely Connected Convolutional Networks) family. It is particularly powerful for image classification tasks and has been successfully applied to various domains, including medical image analysis such as lung disease detection. DenseNet introduces the concept of dense blocks, where each layer in a block receives input from all preceding layers. This densely connected structure promotes feature reuse and facilitates the flow of information throughout the network.

   Neural networks trained on ImageNet can be used as a starting point for training models on medical image datasets. This is known as transfer learning. The lower layers of deep neural networks trained on ImageNet are often capable of learning general features and patterns from images, which can be beneficial for tasks like lung disease detection. In our study ResNet50 and DenseNet-121 are both deep neural network architectures that have been pre-trained on the ImageNet dataset. [32] DenseNet121 and ResNet50 were used in the simulations, and the results showed that the model trained by DenseNet121 had better accuracy than that trained by ResNet50.

Dataset Overview:

We have used the VinBigData Chest X-ray Abnormalities Detection dataset, a crucial resource for a competitive domain in medical image analysis. The dataset comprises 18,000 postero-anterior (PA) chest X-ray scans in DICOM format. Out of these 18,000 we have used approximately 15,000 images due to restrictions on processing power. The dataset's diverse content, precise labeling by experienced radiologists, and inclusion of ground truth data make it instrumental for developing and evaluating algorithms for the classification and localization of thoracic lung diseases and abnormalities.

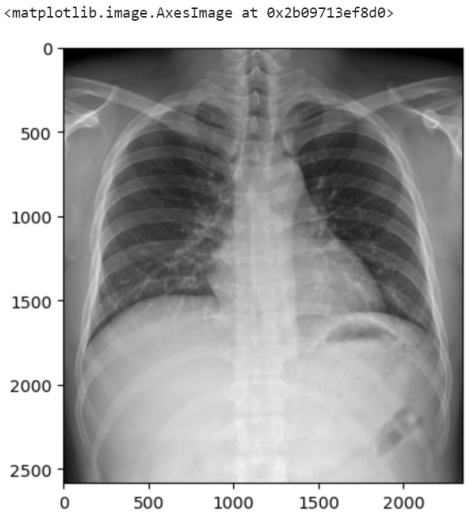

Fig 6: Dataset instance

The Dataset Characteristics are as follows:

1. **Image Format:**

   All images are stored in DICOM format, a standard in medical imaging, offering additional data advantageous for visualization and classification.

2. **Labeling Process:**

   A panel of experienced radiologists extensively labeled each image for the presence of 14 critical radiographic findings, covering a spectrum of thoracic lung diseases and abnormalities. This ensures the dataset's diversity and clinical relevance.

3. **Critical Findings:**

   The dataset includes 14 critical radiographic findings, enumerated as follows:

   - Aortic enlargement
   - Atelectasis
   - Calcification
   - Cardiomegaly
   - Consolidation
   - ILD (Interstitial Lung Disease)
   - Infiltration
   - Lung Opacity
   - Nodule/Mass
   - Other lesion
   - Pleural effusion
   - Pleural thickening
   - Pneumothorax
   - Pulmonary fibrosis

4. **"No Finding" Class:**

   A specific class (class ID 14) designates images without critical findings, allowing for the identification and classification of absence, contributing to a comprehensive dataset.

5. **Radiologist Ground Truth:**

   Ground truth data labeled by multiple radiologists enhances the reliability and accuracy of the dataset, crucial for algorithm development and evaluation.

Dataset Files:

1. Train Set Metadata (train.csv):

This file contains metadata for each object in the training set, including:

- `image_id`: Unique image identifier
- `class_name`: Name of the class of the detected object (or "No finding")
- `class_id`: ID of the class of the detected object
- `rad_id`: ID of the radiologist who made the observation
- `x_min`, `y_min`: Minimum X and Y coordinates of the object's bounding box
- `x_max`, `y_max`: Maximum X and Y coordinates of the object's bounding box
- Some images may contain multiple objects, reflecting real-world clinical complexity.

Methodology:

- **Pre-Processing:**

  In the initial phase of data preprocessing, we acquired a DICOM-formatted dataset from Kaggle, extracting pixel arrays and meticulously adjusting intensities based on DICOM metadata. Subsequent steps included the normalization of pixel values using mean and standard deviation, contributing to data consistency. Contrast stretching, confined within the range of 0 to 255, further refined image quality, setting the stage for subsequent analyses.

  Our meticulous approach continued with image transformations into PIL format, followed by resizing using LANCZOS interpolation for optimal detail preservation. Transformation from greyscale to RGB color space enriched image information, essential for comprehensive analysis. The resulting images, saved in JPEG format, include original contrast-stretched, greyscale-transformed, and RGB-transformed versions. This organized output enhances clarity, accessibility, and reproducibility, aligning with scientific standards for robust dataset preparation.

- **Models Used: (Original and Greyscale)**

  We are first implementing a lightning based model that serves as parent class for the models that we have implemented. The framework is extensible, allowing for the implementation of specific models like XRayResNet50, XRayDenseNet121, MLP, and CustomCNN, each tailored to a particular neural network architecture. Our approach takes images as xray or rgb and assigns weights accordingly. The approach has been kept dynamic, so as to allow testing of various models performances on different data types. The module is designed to handle both binary and multiclass classification tasks based on a provided configuration. The choice of loss function (cross_entropy or dynamically specified) and the number of classes is determined by the configuration. The architecture includes methods for training, validation, and testing steps, with metrics such as loss and accuracy being logged.

  1. **ResNet50:**

     We are using the standard ResNet50 trained on ImageNet. Leveraging the ResNet-50 architecture, a well-established deep neural network for image classification, this class initializes the model with pre-trained weights, thereby harnessing the benefits of transfer learning. To ensure task adaptability, the class incorporates features for handling greyscale input images, modifying the initial convolutional layer accordingly. Furthermore, parameter freezing is employed to maintain the integrity of the pre-trained ResNet-50 while facilitating efficient training on specific classification tasks. The fully connected layer is customized to accommodate the requisite number of output classes, offering versatility in addressing diverse classification scenarios. This tailored implementation encapsulates the inherent flexibility and adaptability of the proposed framework, showcasing its applicability in the context of X-ray image analysis in medical research. The model takes images in greyscale and it modifies the first convolutional layer (conv1). It replaces the original layer with a new layer that takes a single-channel (greyscale) input and initializes its weights based on the mean of the original weights across channels.

2. **DenseNet 121:**

Next we are employing the DenseNet-121 architecture, renowned for its effectiveness in deep learning-based image analysis, the class initializes the model with pre-trained weights to capitalize on transfer learning benefits. Parameter freezing is applied to maintain the integrity of the pre-trained DenseNet-121 while facilitating task-specific adaptations. Notably, the class accommodates greyscale input images, dynamically modifying the initial convolutional layer (conv0) to process single-channel inputs. This adaptability ensures versatility in handling diverse image datasets. Furthermore, the fully connected layer (classifier) is customized to reflect the number of output classes specified in the configuration, emphasizing the flexibility of the proposed framework. The comprehensive implementation encapsulates the sophistication and adaptability required for accurate and efficient X-ray image classification tasks, underscoring its relevance in medical image analysis and contributing to the broader landscape of deep learning applications in healthcare.

- x as the input tensor.

- W_i and b_i as the weights and biases of layer \(i \), respectively.

- ReLU(x) as the rectified linear unit activation function.

- The forward pass through the DenseNet-121 model can be expressed mathematically as follows:
  - Initial Convolutional Layer (for greyscale input):
  - $x_0 = Conv2D_{greyscale}(x, W_0, b_0)$

- Dense Blocks and Transition Layers:
  - DenseNet-121 consists of dense blocks, which are groups of densely connected layers, and transition layers that downsample feature maps. These operations can be represented as:
  - $x_i = DenseBlock_i(x_i, w_i, b_i)$
  - $x_i = TransitionLayer_i(x_i, w_i, b_i)$

- Global Average Pooling:
  - The output from the final dense block is followed by a global average pooling operation:
  - $x_{gap} = GlobalAvgPool(x_{final\_dense\_block})$

- Fully Connected Layer (Classifier):
  - The global average-pooled feature map is then fed into the fully connected layer (classifier) to obtain the final output logits:
  - $logits = x_{gap} * W_{classifier} + b_{classifier}$

- Softmax Activation (for Multiclass Classification):

- If the classification task is multiclass, a softmax activation is applied to obtain class probabilities:
- $probabilities = Softmax(logits)$

3. **MLP:**

The MLP class, an integral component of the proposed X-ray image classification framework. This class is designed to encapsulate a Multilayer Perceptron (MLP) architecture for the classification of X-ray images. It extends the abstract XRayBasemodel framework, incorporating modularity and flexibility. The initialization process is conditioned on the user-specified configuration, particularly addressing whether the input channels are greyscale or RGB. For greyscale images, the input dimensionality is set to one, while for RGB images, it is configured to three. The MLP architecture itself comprises three fully connected layers with rectified linear unit (ReLU) activation functions, interspersed with dropout layers for regularization. The first hidden layer has 512 units, followed by a layer with 256 units, ultimately leading to an output layer with dimensions aligned with the specified number of output classes. This architecture reflects a sequential composition of operations, commencing with data flattening and culminating in class predictions. The incorporation of dropout layers enhances the network's generalization capabilities. The class's versatility renders it suitable for a variety of X-ray image classification tasks, as dictated by the user-defined configuration.

4. **Custom CNN:**

The last model used for comparison is a custom CNN class. Functioning as an essential component within the overarching XRayBasemodel framework, this class is designed to accommodate diverse X-ray image classification tasks through the implementation of a custom Convolutional Neural Network (CNN). The initialization process is contingent upon the user-specified configuration, discerning whether the input channels are greyscale or RGB. For greyscale inputs, the architecture is configured to process a single channel, while for RGB inputs, it is configured for three channels. The CNN architecture is meticulously defined as a sequence of convolutional, activation, pooling, flattening, and fully connected layers. The convolutional layers are followed by Rectified Linear Unit (ReLU) activation functions and max-pooling operations to capture hierarchical features in the input data. The fully connected layers at the end of the network facilitate the mapping of learned features to the specified number of output classes. Importantly, weight initialization is performed to ensure effective training, employing Kaiming normal initialization for convolutional layers and Xavier normal initialization for fully connected layers. The dropout layer is incorporated for regularization, enhancing the model's generalization capabilities. The versatility of the CustomCNN class, reflected in its adaptability to different image modalities and classification tasks, underscores its significance within our proposed methodology.

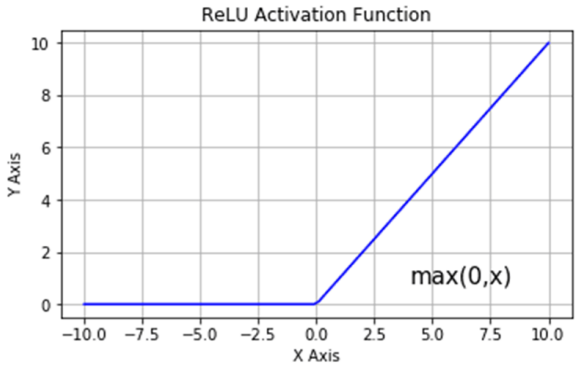

Fig 7: The ReLU activation function [33]

Experimentation:

- **Different Splits:**
  - In our comprehensive evaluation of the dataset, we conducted rigorous testing employing two distinct models: the renowned DenseNet and ResNet50, as well as a combination of ResNet50 and DenseNet121. This multi-model approach allowed us to thoroughly explore the dataset's characteristics and draw robust conclusions.
  - A pivotal aspect of our investigation centered around the unique feature of rad_id, signifying the identifier of the radiologist responsible for making the predictions. Recognizing the potential influence of individual radiologists' biases on the dataset, we treated each radiologist as a distinct distribution, thereby establishing that images are only Independent and Identically Distributed (IID) when considered within the context of a specific radiologist.
  - To address this nuanced consideration, our training protocols encompassed two distinct scenarios. Firstly, we trained our models on datasets where the diagnosis was exclusively made by the same radiologist, preserving the inherent distribution associated with individual practitioners. Subsequently, we explored scenarios where models were trained without regard to rad_id, thereby assessing the performance in a more generalized context.
  - This meticulous approach not only acknowledges the individualized biases introduced by different radiologists but also highlights the importance of understanding and accounting for these biases in the training process. By presenting our findings in this manner, we contribute to the broader discourse on model robustness and the interpretability of results in the context of medical image analysis.

Results:

- Based on the various splits and the models used, the results we found were as follows:

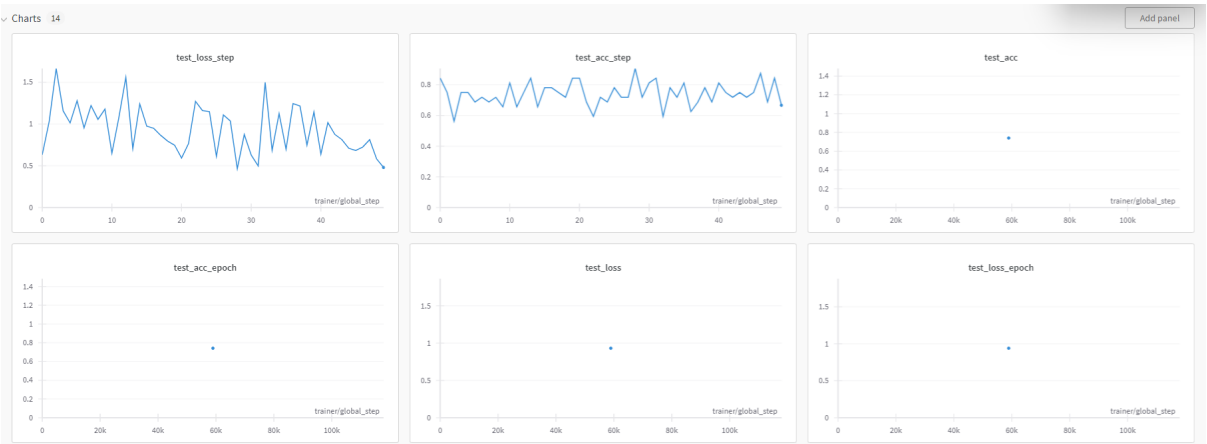

Fig 8: ResNet50_R9_only_full - ResNet50 model on entire dataset having predictions only by the radiologist with the rad_id of 9.

- Here, we achieved a test_acc of 0.756 and test_acc per epoch of 0.751.
- We also achieved a val_acc of 0.73

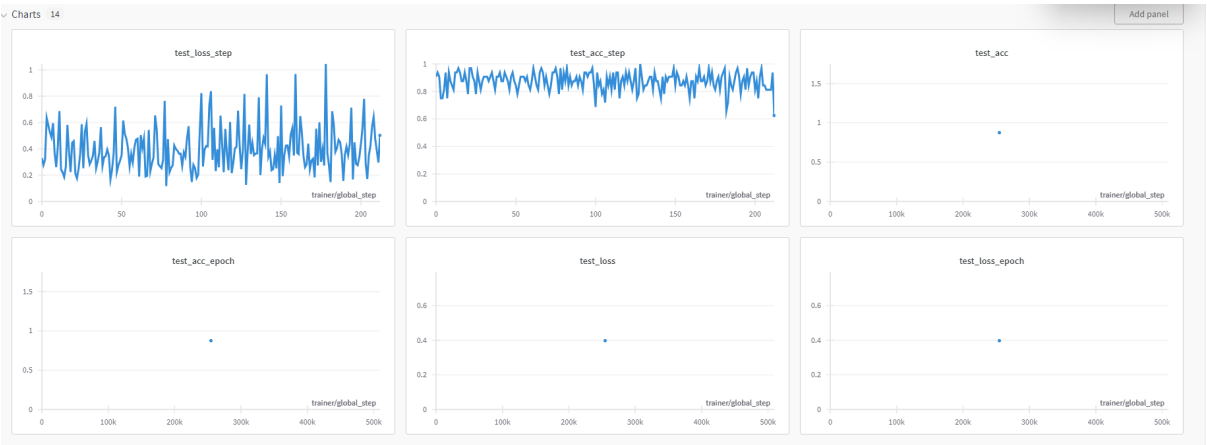

Fig 9: ResNet50_all_rad - ResNet50 model on entire dataset having all predictions ignoring the rad_id.

- Here, we achieved a test_acc 0.874 and a val_acc of 0.883

Fig 10: DenseNet121_R9

- Here, we got a val_acc of 0.38
- All of the results are available in wandb [34].

Conclusion:

In conclusion, this research addresses the challenging task of lung disease detection using neural networks, presenting a comprehensive comparative study of various model architectures. The study focuses on critical lung abnormalities, leveraging a diverse dataset of high-resolution X-ray images. Convolutional Neural Networks (CNNs), Multilayer Perceptrons (MLPs), and pretrained models like ResNet50 and DenseNet121 are evaluated, with a detailed exploration of their performance and efficiency. The paper emphasizes the complexities of medical image classification, particularly in the context of smaller datasets and the intricate nature of anatomical variations. The proposed models, including ResNet50 and DenseNet121, demonstrate adaptability and efficacy in classifying diverse lung diseases, showcasing their potential for enhancing predictive performance in clinical settings.

References:

1) https://my.clevelandclinic.org/health/diseases/16742-aorta-aortic-aneurysm
2) https://emedicine.medscape.com/article/418480-overview?form=fpf
3) D.G. Peroni, A.L. Boner, Atelectasis: mechanisms, diagnosis and management, Paediatric Respiratory Reviews, Volume 1, Issue 3, 2000, Pages 274-278, ISSN 1526-0542, https://doi.org/10.1053/prrv.2000.0059.
4) Jones J, Weerakkody Y, Worsley C, et al. Atelectasis (summary). Reference article, Radiopaedia.org (Accessed on 10 Dec 2023) https://doi.org/10.53347/rID-51373
5) Giachelli, Cecilia M.. Vascular Calcification Mechanisms. Journal of the American Society of Nephrology 15(12):p 2959-2964, December 2004. | DOI: 10.1097/01.ASN.0000145894.57533.C4
6) Weerakkody Y, Niknejad M, Bell D, et al. Pulmonary calcification. Reference article, Radiopaedia.org (Accessed on 10 Dec 2023) https://doi.org/10.53347/rID-52343
7) Amin H, Siddiqui WJ. Cardiomegaly. [Updated 2022 Nov 20]. In: StatPearls [Internet]. Treasure Island (FL): StatPearls Publishing; 2023 Jan-. Available from: https://www.ncbi.nlm.nih.gov/books/NBK542296/
8) Radswiki T, Niknejad M, Suyama D, et al. Cardiomegaly. Reference article, Radiopaedia.org (Accessed on 10 Dec 2023) https://doi.org/10.53347/rID-12661
9) https://www.healthline.com/health/lung-consolidation
10) https://www.lung.org/lung-health-diseases/lung-disease-lookup/interstitial-lung-disease
11) Jones J, Abdulmanan M, Weerakkody Y, et al. Interstitial lung disease. Reference article, Radiopaedia.org (Accessed on 10 Dec 2023) https://doi.org/10.53347/rID-14479
12) Weerakkody Y, Bell D, Pulmonary infiltrates. Reference article, Radiopaedia.org (Accessed on 10 Dec 2023) https://doi.org/10.53347/rID-25581
13) Türk F, Kökver Y. Detection of Lung Opacity and Treatment Planning with Three-Channel Fusion CNN Model. Arab J Sci Eng. 2023 Apr 14:1-13. doi: 10.1007/s13369-023-07843-4. Epub ahead of print. PMID: 37361471; PMCID: PMC10103673.
14) Jones J, Knipe H, Botz B, et al. Pulmonary nodule. Reference article, Radiopaedia.org (Accessed on 10 Dec 2023) https://doi.org/10.53347/rID-10187

15) Krishna R, Antoine MH, Rudrappa M. Pleural Effusion. [Updated 2023 Mar 18]. In: StatPearls [Internet]. Treasure Island (FL): StatPearls Publishing; 2023 Jan-. Available from: https://www.ncbi.nlm.nih.gov/books/NBK448189/
16) Jones J, Silverstone L, Ismail M, et al. Pleural effusion. Reference article, Radiopaedia.org (Accessed on 10 Dec 2023) https://doi.org/10.53347/rID-6159
17) https://www.mesotheliomahub.com/mesothelioma/pleural-thickening/
18) https://www.mayoclinic.org/diseases-conditions/pneumothorax/symptoms-causes/syc-20350367
19) Gorrochategui M, Ramsey, MD A, Niknejad M, et al. Pneumothorax. Reference article, Radiopaedia.org (Accessed on 10 Dec 2023) https://doi.org/10.53347/rID-4578
20) https://www.healthdirect.gov.au/pulmonary-fibrosis
21) Weerakkody Y, Niknejad M, Yadegarfar M, et al. Pulmonary fibrosis. Reference article, Radiopaedia.org (Accessed on 10 Dec 2023) https://doi.org/10.53347/rID-22678
22) Meha Desai, Manan Shah, An anatomization on breast cancer detection and diagnosis employing multi-layer perceptron neural network (MLP) and Convolutional neural network (CNN), Clinical eHealth, Volume 4, 2021 Pages 1-11, ISSN 2588-9141, https://doi.org/10.1016/j.ceh.2020.11.002.
23) V. Kadali, B. S. Pudi, K. A. Shaik, A. Janjam and J. Javvadi, "Pneumonia Detection in Chest X-Ray Images by using Resnet-50 Deep Learning Algorithm," *2023 Third International Conference on Artificial Intelligence and Smart Energy (ICAIS)*, Coimbatore, India, 2023, pp. 1078-1084, doi: 10.1109/ICAIS56108.2023.10073748.
24) Sriporn, K.; Tsai, C.-F.; Tsai, C.-E.; Wang, P. Analyzing Lung Disease Using Highly Effective Deep Learning Techniques. *Healthcare* **2020**, *8*, 107. https://doi.org/10.3390/healthcare8020107
25) Sharma S, Guleria K. A comprehensive review on federated learning based models for healthcare applications. Artif Intell Med. 2023 Dec;146:102691. doi: 10.1016/j.artmed.2023.102691. Epub 2023 Oct 30. PMID: 38042608.
26) Huang, Z., Liu, X., Wang, R., Zhang, M., Zeng, X., Liu, J., Yang, Y., Liu, X., Zheng, H., Liang, D., et al. (2021). Fanet: fast assessment network for the novel coronavirus (covid-19) pneumonia based on 3d ct imaging and clinical symptoms. Applied Intelligence, 51:2838–2849.
27) Jakhar, K. and Hooda, N. (2018). Big data deep learning framework using keras: A case study of pneumonia prediction. In 2018 4th International Conference on computing communication and automation (ICCCA), pages 1–5. IEEE.
28) Deng, J., Dong, W., Socher, R., Li, L.-J., Li, K., and Fei-Fei, L. (2009). Imagenet: A large-scale hierarchical image database. In 2009 IEEE conference on computer vision and pattern recognition, pages 248–255. Ieee.
29) Zhuang, F., Qi, Z., Duan, K., Xi, D., Zhu, Y., Zhu, H., Xiong, H., and He, Q. (2020). A comprehensive survey on transfer learning. Proceedings of the IEEE, 109(1):43–76.
30) El Asnaoui, K., Chawki, Y., and Idri, A. (2021). Automated methods for detection and classification pneumonia based on x-ray images using deep learning. In Artificial intelligence and blockchain for future cybersecurity applications, pages 257–284. Springer.
31) I. Chouat, A. Echtioui, R. Khemakhem, W. Zouch, M. Ghorbel and A. B. Hamida, "Lung Disease Detection in Chest X-ray Images Using Transfer Learning," 2022 6th International Conference on Advanced Technologies for Signal and Image Processing (ATSIP), Sfax, Tunisia, 2022, pp. 1-6, doi: 10.1109/ATSIP55956.2022.9805892.

32) Fan R, Bu S. Transfer-Learning-Based Approach for the Diagnosis of Lung Diseases from Chest X-ray Images. Entropy (Basel). 2022 Feb 22;24(3):313. doi: 10.3390/e24030313. PMID: 35327823; PMCID: PMC8947580.

33) https://www.nomidl.com/deep-learning/difference-between-leaky-relu-and-relu-activation-function/

34) https://wandb.ai/aml_iu/applied%20machine%20learning